Intraretinal stimulation with high density carbon fiber microelectrodes

Dorsa Haji Ghaffari
Biomedical Engineering
University of Michigan
Ann Arbor MI, USA
ghdor@umich.edu

Elena Della Valle
Biomedical Engineering
University of Michigan
Ann Arbor MI, USA
eldellav@umich.edu

Paras R. Patel
Biomedical Engineering
University of Michigan
Ann Arbor MI, USA
parasp@umich.edu

Julianna Richie
Biomedical Engineering
University of Michigan
Ann Arbor MI, USA
jmrichie@umich.edu

Joseph G. Letner
Biomedical Engineering
University of Michigan
Ann Arbor MI, USA
letnerj@umich.edu

Cynthia A. Chestek
Biomedical Engineering
University of Michigan
Ann Arbor MI, USA
cchestek@umich.edu

James D. Weiland
Biomedical Engineering
University of Michigan
Ann Arbor MI, USA
weiland@umich.edu

2023 11th International IEEE/EMBS Conference on Neural Engineering (NER) | 978-1-6654-6292-1/23/$31.00 ©2023 IEEE | DOI: 10.1109/NER52421.2023.10123735

***Abstract*—Retinal prostheses can improve vision for patients blinded by photoreceptor degenerative diseases. Despite the benefits of artificial vision, low spatial resolution of these prostheses limits the positive impact of clinically available devices. Visual percepts generated by single electrodes in epiretinal and subretinal implants can overlap and result in an unclear image, which limits shape and letter perception for retinal prosthesis users. However, research suggests higher resolution may be possible with smaller electrodes implanted intraretinally, in close proximity of target neurons. In this study we used penetrating subcellular-scale carbon fiber microelectrodes for retinal stimulation in an *ex vivo* mouse retina, and performed calcium imaging to record spatial activation of retinal ganglion cells (RGC) in response to different stimulation amplitudes and RGC-electrode distances. We observed smaller RGC spatial activities and less off-target stimulation with higher RGC-electrode distances, which may be an indication of indirect RGC activation through bipolar cells. Impedance measurements of carbon fiber electrodes demonstrated their mechanical and electrical stability throughout the process of insertion and stimulation. Our results indicate that modification of pulse amplitudes and electrode depths can create small and focal responses around the active electrode. Intraretinal stimulation with carbon fibers can potentially increase stimulation precision and image resolution for retinal prostheses in clinical applications.**

Keywords—retinal prosthesis, intraretinal stimulation, carbon fiber, calcium imaging, retinal ganglion cell

I. Introduction

Retinal implants can partially restore vision for patients blinded by outer retinal degenerative diseases such as age-related macular degeneration and retinitis pigmentosa [1], [2]. The best visual acuity achieved by subretinal and epiretinal implants are 20/460 [3] and 20/1260 [4] respectively, which are lower than the legal blindness acuity of 20/200. Epiretinal prosthesis users report elongated percepts due to unintended stimulation of axons which activates off-target retinal ganglion cells (RGCs) [5]. Electrode location relative to axon trajectories can affect percept shape and cause inconsistencies between phosphenes [6]. Subretinal implants can achieve higher visual acuities by preferentially activating bipolar cells and avoiding axonal activation. However, photovoltaic subretinal implants have a pixel diameter of 100 µm, and there are limits to decreasing the pixel size and increasing the image resolution [7], [8]. We used subcellular-scale carbon fiber microelectrodes for intraretinal stimulation to achieve higher stimulation precisions.

Research supported by National Science Foundation (NSF 1707316), National Institutes of Health (T32 EY013934), and University of Michigan.

II. Methods

A. Electrode array fabrication

High density carbon fiber (HDCF) electrode arrays with four fibers each were fabricated [9]. Arrays had sharpened CF tips of 50 µm length (surface area of ~ 1000 µm^2). A platinum-iridium (PtIr) alloy was electrodeposited on the tips to enable microstimulation without material degradation [10], [11] (Fig. 1).

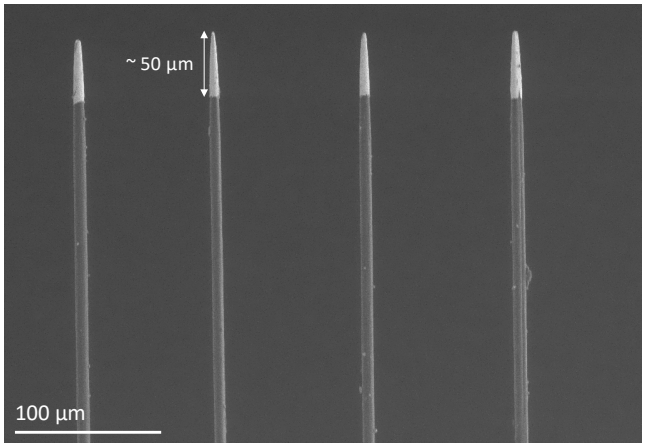

Figure 1: SEM image of an HDCF electrode array with 4 fibers. Fiber tip exposure is ~ 50 µm. Tips are sharpened and coated with Pt-Ir.

B. AAV injection and ex vivo setup

Wild-type mice C57BL/6 were used in this study and all procedures were approved by the Institutional Animal Care and

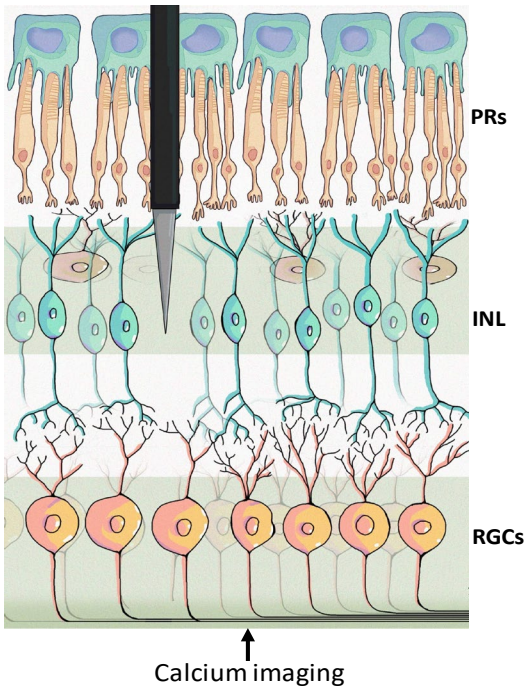

Figure 2: Schematic of the stimulation and recording setup. Carbon fibers are inserted from the photoreceptor side and calcium imaging is done from the RGC side. Figure is drawn to scale. (illustration by Muru Zhou, muruzhou.com)

Use Committee (IACUC) and the Institutional Biosafety Committee (IBC) at the University of Michigan. An adeno-associated virus (AAV) vector, rAAV2-CAG-GCaMP6f-WPRE-bGH, was injected intravitreally to induce GCaMP6f expression in mouse RGCs [12]. 3-4 weeks after injection, animals were anesthetized with ketamine (100 mg kg^{-1}) and xylazine (10 mg kg^{-1}). Eyes were enucleated and retinas were isolated inside a perfusion chamber with bicarbonate-buffered Ames' Medium (Sigma-Aldrich, St. Louis, MO). After removing both eyes animals were euthanized by CO_2 overdose. Retinas were mounted on a transparent chamber with RGCs facing down to allow for calcium imaging. During the experiment retina was superfused with bicarbonate-buffered Ames' Medium adjusted to 280 mOsm, bubbled with 95% O_2 – 5% CO_2 gas, and kept at 33 °C. HDCFs were inserted from the subretinal (photoreceptor) side and positioned at different distances relative to the RGC layer using a micromanipulator.

C. Electrical stimulation and calcium imaging

Electrical stimulation consisted of cathodic-first biphasic pulses of 0.5 ms duration, generated by the PlexStim electrical stimulator system (Plexon Inc., Dallas, Texas). Stimulation was delivered at 120 Hz frequency to evoke multiple spikes and a detectable calcium transient [13]. Various stimulation amplitudes (1 – 10 µA) and RGC-electrode distances (20, 70, and 100 µm) were examined in each retinal region and RGC spatial activity was recorded. Calcium images were captured by an electron-multiplied charge-coupled device (EMCCD) camera (iXon 897, Andor Technology, Belfast, Northern Ireland) through an Olympus UPLFLN 0.3 numerical aperture (NA) 20× objective at 10 Hz. Fluorescence images were recorded before and during stimulation and RGC spatial activity was obtained by subtracting the baseline from the

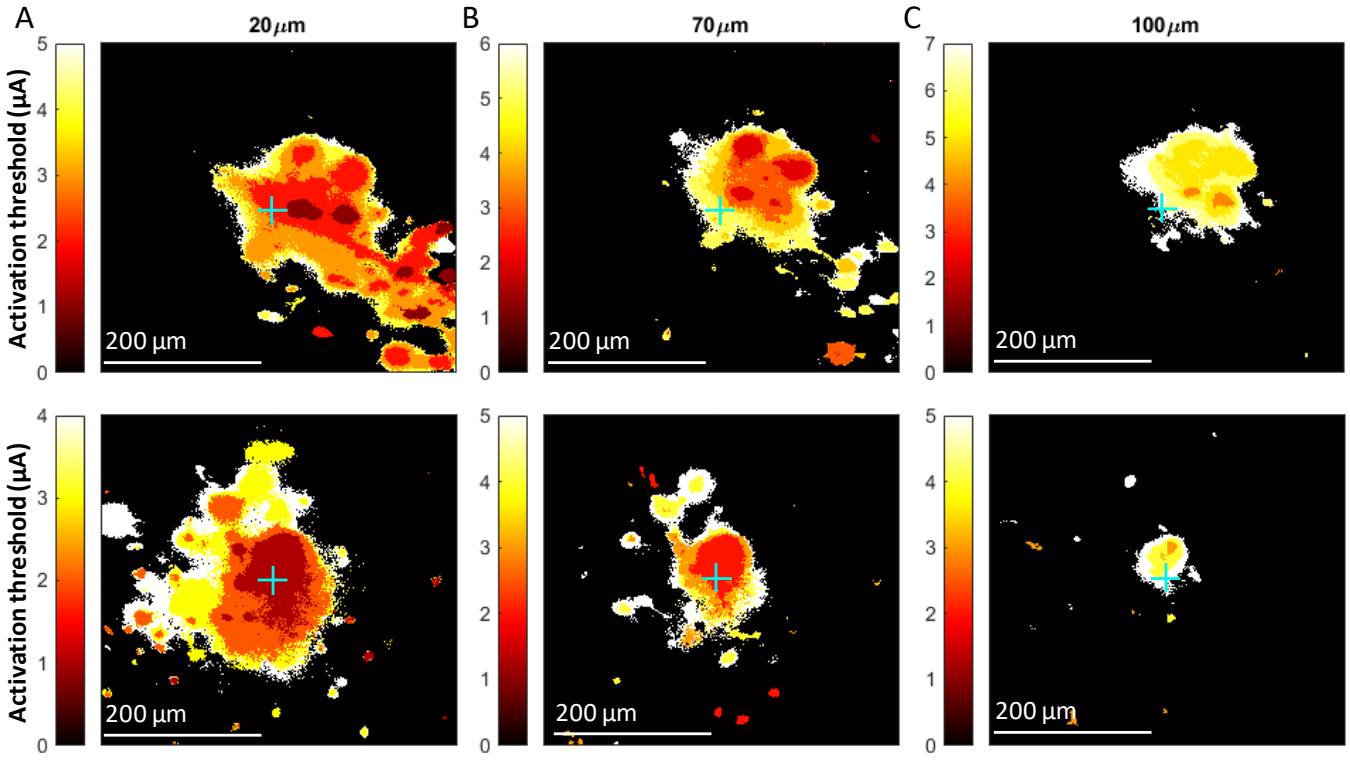

Figure 3: RGC spatial activity in response to intraretinal electrical stimulation. Heat map shows pixel activation thresholds in µA. RGC-electrode distance is A) 20 µm, B) 70 µm, C) 100 µm. Electrode tip location is marked with a blue cross in the center.

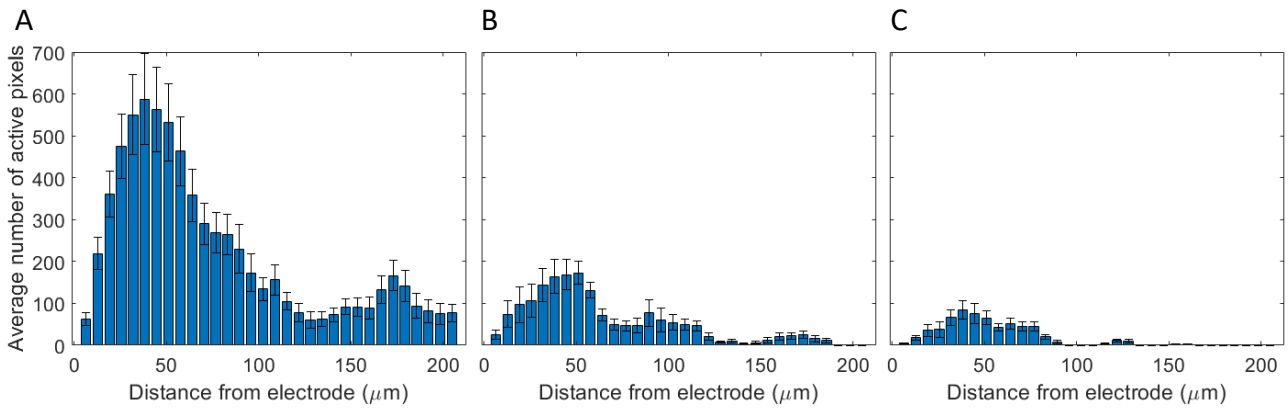

Figure 4: Histogram of average number of active pixels (n = 10) binned over distance from the electrode (bin size = 8 pixels) at threshold current amplitudes at A) 20 µm, B) 70 µm, and C) 100 µm RGC-electrode distance.

stimulation images. The result (ΔF) was further normalized relative to baseline (F) to remove noise in the fluorescent signal ($\Delta F/F > 15\%$). Activation threshold is the current amplitude at which $\Delta F/F > 15\%$ in a given region.

III. Results

Figure 3 shows example RGC spatial activity in two different retinal regions, with electrode tip positioned at 20, 70, and 100 µm away from the RGCs. At 20 µm RGC-electrode distance, RGCs were consistently activated at 1 µA amplitude with 0.5 ms pulse width. Amplitude could not be lowered due to the stimulator resolution; thus the evoked calcium transients were likely suprathreshold at 1 µA. Average current threshold at 70 and 100 µm RGC-electrode distances was 2.5 µA and 4.3 µA respectively (n =10), which are 43.2% and 2.3% lower than the average threshold with epiretinal stimulation in a similar setup [12]. The 1 µA stimulus amplitude at 20 µm RGC-electrode distance is 77.2% lower than the average epiretinal threshold.

To quantify RGC spatial activity as a function of electrode depth and current amplitude, active pixels at threshold current were binned over distance from electrode with a bin size of 8 pixels (1 pixel = 800 nm) (Fig. 4). We observe a higher number of active pixels, and more off-target activation with lower RGC-electrode distances, with the caveat that the minimum current output of 1 µA resulted in suprathreshold stimulation at 20 µm RGC-electrode distance.

Figure 5 shows impedance measurement data for a single carbon fiber before stimulation and after stimulation. This indicates that the CF electrode was not damaged by insertion into retina or stimulation.

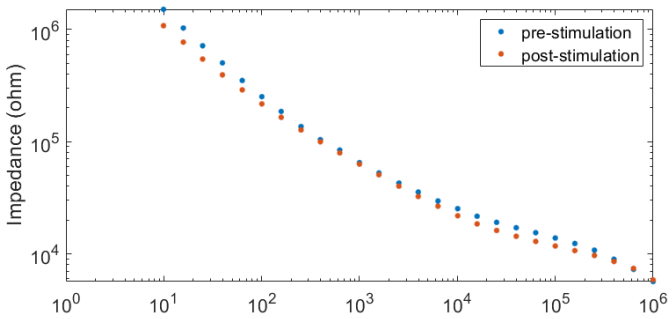

Figure 5: Impedance measurement for a single carbon fiber before and after stimulation.

IV. Discussion

We have demonstrated the feasibility of RGC stimulation with intraretinal carbon fiber microelectrodes. Low precision of stimulation remains a problem with current retinal prostheses, which limits shape and letter perception. Precisely stimulating target neurons and minimizing off-target stimulation is crucial to create non-overlapping percepts and high resolution images. Visual acuity has been correlated to two-point resolution, which depends on the distance between two discernible phosphenes [14].

Previous studies have shown that changing pulse width, pulse type, amplitude, and RGC-electrode distance affects RGC spatial activity and stimulation thresholds [12], [15]–[18], and electrode-specific optimization of stimulation parameters can help achieve more focal activation [15]. However, these approaches can be limited by electrode size and density. This study shows the possibility of creating small activation areas around the electrode using penetrating carbon fiber microelectrodes. RGC spatial activities were smaller and activation thresholds were lower compared to epiretinal stimulation in a similar setup [12]. Manipulating pulse amplitude and RGC-electrode distance affected the RGC spatial activity. We also observed that RGC spatial activity varies in different retinal regions in response to the same stimulation settings (Fig. 3). This inconsistency could be due to complex axonal pathways and relative location to the optic disc.

The carbon fiber electrodes had a geometric surface area of 1000 µm^2. The lowest current threshold was 1 µA (0.5 nC) and highest current threshold was 8 µA (4 nC) (at 100 µm RGC-electrode distance). Therefore, charge density threshold is 0.05 mC/cm^2 – 0.4 mC/cm^2, which is within the range of safe charge density for these materials [19].

Several recent studies have explored using intraretinal penetrating electrodes to improve precision of retinal stimulation. Ganesan *et al.* fabricated a diamond penetrating electrode array containing cylindrical electrodes, but most electrodes conformably distorted the rat retina instead of penetrating it, possibly due to the cylinders' blunt tips [20].

Rincón Montes *et al.* developed bidirectional electrode arrays made with flexible polymers; the electrodes were 140–225 µm long, 50–100 µm wide and 3–7 µm thick, with a 25µm-diameter disc electrode [21]. They could record from certain retinal neurons *in vitro*, but stimulation was not attempted. Flores *et al.* fabricated and implanted two types of pillar electrodes in the subretinal space in rats, (22µm height, 6µm diameter, 40µm pitch) and electroplated gold pillars with dome-shaped caps (10µm height, 10µm dome diameter, 40µm pitch). Six weeks post-surgery, retinal tissue had migrated into the inter-electrode space, with no visible gliosis, but no stimulation was performed [22]. Chen *et al.* report the results of chronic, passive intraretinal arrays implanted subretinally in Yucatan Minipig [23]. The pillar electrodes had 30µm diameter and 200µm spacing (20/800 visual acuity). Optical coherence tomography (OCT) confirmed pillar penetration into the retina. The NR600, which has been implanted in 9 people in a clinical trial, is an experimental retinal prosthesis with an intraretinal array positioned on the epiretinal side [24]. NR600 electrodes are spaced 100 µm apart, equating to 20/400 [25].

Future work includes refining pulse parameters and RGC-electrode distance and generating activation patterns with multi-electrode stimulation. Inner retinal layers can go through morphological changes secondary to photoreceptor degeneration [26], and a heterogeneous degeneration can lead to more variability in RGC response among different retinal regions. In addition, outer retinal thickness decreases with photoreceptor degeneration [27], so it is important to optimize electrode depth with rd10 mice in the future. To determine the cellular target of intraretinal stimulation with different electrode depths, synaptic blockers will be used to isolate RGCs in future experiments. Carbon fibers have shown exceptional performance in applications that require precise positioning, and have proven to be flexible during small mechanical stimuli [28], [29]. However, Long-term safety should be investigated through chronic implantation of carbon fibers *in vivo*.

REFERENCES

[1] J. D. Weiland and M. S. Humayun, "Retinal prosthesis," *IEEE Trans. Biomed. Eng.*, vol. 61, no. 5, pp. 1412–1424, 2014.

[2] E. Zrenner, "Fighting blindness with microelectronics," *Science Translational Medicine*. 2013.

[3] M. S. Humayun *et al.*, "Interim results from the international trial of second sight's visual prosthesis," *Ophthalmology*, 2012.

[4] D. Palanker, Y. Le Mer, S. Mohand-Said, and J. A. Sahel, "Simultaneous perception of prosthetic and natural vision in AMD patients," *Nat. Commun. 2022 131*, vol. 13, no. 1, pp. 1–6, Jan. 2022.

[5] D. Nanduri *et al.*, "Frequency and amplitude modulation have different effects on the percepts elicited by retinal stimulation," *Investig. Ophthalmol. Vis. Sci.*, 2012.

[6] M. Beyeler, D. Nanduri, J. D. Weiland, A. Rokem, G. M. Boynton, and I. Fine, "A model of ganglion axon pathways accounts for percepts elicited by retinal implants," *Sci. Rep.*, 2019.

[7] E. Ho *et al.*, "Photovoltaic implant simulator reveals resolution limits in subretinal prosthesis," *J. Neural Eng.*, vol. 19, no. 5, p. 055008, Sep. 2022.

[8] E. Ho *et al.*, "Pixel size limit of the PRIMA implants: from humans to rodents and back," *J. Neural Eng.*, vol. 19, no. 5, p. 055003, Sep. 2022.

[9] Y. Huan *et al.*, "Carbon fiber electrodes for intracellular recording and stimulation," *J. Neural Eng.*, vol. 18, no. 6, p. 066033, Dec. 2021.

[10] E. della Valle *et al.*, "Electrodeposited Platinum Iridium Enables Microstimulation With Carbon Fiber Electrodes," *Front. Nanotechnol.*, vol. 3, p. 91, Dec. 2021.

[11] E. Della Valle, E. J. Welle, C. A. Chestek, and J. D. Weiland, "Compositional and morphological properties of platinum-iridium electrodeposited on carbon fiber microelectrodes," *J. Neural Eng.*, vol. 18, no. 5, Oct. 2021.

[12] Y. C. Chang, D. H. Ghaffari, R. H. Chow, and J. D. Weiland, "Stimulation strategies for selective activation of retinal ganglion cell soma and threshold reduction," *J. Neural Eng.*, 2019.

[13] A. C. Weitz *et al.*, "Imaging the response of the retina to electrical stimulation with genetically encoded calcium indicators," *J. Neurophysiol.*, 2013.

[14] Thomas Z. Lauritzen, D. Nanduri, J. Weiland, J. D. Dorn, K. McClure, and R. Greenberg;, "Inter-electrode Discriminability Correlates With Spatial Visual Performance In ArgusTM II Subjects," *IOVS*, vol. 52, no. 14, p. 4927, 2011.

[15] D. Haji Ghaffari, A. D. Akwaboah, E. Mirzakhalili, and J. D. Weiland, "Real-Time Optimization of Retinal Ganglion Cell Spatial Activity in Response to Epiretinal Stimulation," *IEEE Trans. Neural Syst. Rehabil. Eng.*, 2021.

[16] A. C. Weitz *et al.*, "Improving the spatial resolution of epiretinal implants by increasing stimulus pulse duration," *Sci. Transl. Med.*, vol. 7, no. 318, 2015.

[17] D. Haji Ghaffari *et al.*, "The effect of waveform asymmetry on perception with epiretinal prostheses," *J. Neural Eng.*, 2020.

[18] A. K. Ahuja *et al.*, "Factors Affecting Perceptual Threshold in Argus II Retinal Prosthesis Subjects," *Transl. Vis. Sci. Technol.*, 2013.

[19] S. F. Cogan, "Neural stimulation and recording electrodes," *Annual Review of Biomedical Engineering*. 2008.

[20] K. Ganesan *et al.*, "Diamond penetrating electrode array for epi-retinal prosthesis," *Annu. Int. Conf. IEEE Eng. Med. Biol. Soc. IEEE Eng. Med. Biol. Soc. Annu. Int. Conf.*, vol. 2010, pp. 6757–6760, 2010.

[21] V. Rincón Montes *et al.*, "Development and in vitro validation of flexible intraretinal probes," *Sci. Reports 2020 101*, vol. 10, no. 1, pp. 1–14, Nov. 2020.

[22] T. Flores *et al.*, "Optimization of pillar electrodes in subretinal prosthesis for enhanced proximity to target neurons," *J. Neural Eng.*, vol. 15, no. 3, p. 036011, Mar. 2018.

[23] J. Chen *et al.*, "Implantation and Extraction of Penetrating Electrode Arrays in Minipig Retinas," *Transl. Vis. Sci. Technol.*, vol. 9, no. 5, pp. 19–19, Apr. 2020.

[24] L. Yanovitch, D. Raz-Prag, and Y. Hanein, "A new high-resolution three-dimensional retinal implant: System design and preliminary human results," *bioRxiv*, p. 2022.09.14.507901, Sep. 2022.

[25] D. Palanker, A. Vankov, P. Huie, and S. Baccus, "Design of a high-resolution optoelectronic retinal prosthesis," in *Journal of Neural Engineering*, 2005.

[26] E. Strettoi, V. Pignatelli, C. Rossi, V. Porciatti, and B. Falsini, "Remodeling of second-order neurons in the retina of rd/rd mutant mice," *Vision Res.*, vol. 43, no. 8, pp. 867–877, 2003.

[27] M. E. Pennesi *et al.*, "Long-Term Characterization of Retinal Degeneration in rd1 and rd10 Mice Using Spectral Domain Optical Coherence Tomography," *Invest. Ophthalmol. Vis. Sci.*, vol. 53, no. 8, pp. 4644–4656, Jul. 2012.

[28] A. A. Jiman *et al.*, "Multi-channel intraneural vagus nerve recordings with a novel high-density carbon fiber microelectrode array," *Sci. Reports 2020 101*, vol. 10, no. 1, pp. 1–13, Sep. 2020.

[29] Y. Huan *et al.*, "Carbon fiber electrodes for intracellular recording and stimulation," *J. Neural Eng.*, vol. 18, no. 6, Dec. 2021.